MODELING THE BEHAVIOR OF A HOMOPOLAR MOTOR

A Thesis presented to the Faculty of the Graduate School

University of Missouri-Columbia

In Partial Fulfillment

Of the Requirements for the Degree

Master of Science

By

GIANETTA MARIA BELARDE

Dr. Thomas G. Engel, Thesis Supervisor

December 2008

The undersigned, appointed by the dean of the Graduate School, have examined the thesis entitled

MODELING THE BEHAVIOR OF A HOMOPOLAR MOTOR

presented by Gianetta Belarde

a candidate for the degree of Master of Science in Electrical Engineering

and hereby certify that, in their opinion, it is worthy of acceptance.

_____

Professor Thomas Engel

_____

Professor John Farmer

_____

Professor John Gahl

_____

Acknowledgements

I would like to extend my deepest gratitude to my advisor and mentor, Dr. Thomas G. Engel. His motivation and insight provided me with the guidance to finish this project, and for that I will always be grateful to him.

I would also like to thank several individuals who have provided me with guidance and support throughout my academic career, especially Prof. Michael Devaney, Prof. Robert O'Connell, Prof. Alex Iosevich, Dr. Jim Fischer, Dr. Gregory Triplett, and Dr. Guilherme DeSouza. Additionally, I would like to thank the other two members of my thesis committee, Dr. John Gahl and John Farmer.

Finally, I wish to dedicate this work to my loving parents. Their lifelong support and caring has been instrumental in my life.

MODELING THE BEHAVIOR OF A HOMOPOLAR MOTOR

Gianetta Maria Belarde

Dr. Thomas G. Engel, Thesis Supervisor

ABSTRACT

The design, construction, and operating characteristics of a homopolar motor are described in this thesis using both physical experimentation and simulation software. This type of motor converts electrical energy into mechanical energy using the Lorentz force. The torque from this force is used to propel the homopolar motor forward. The nickel-metal hydride batteries used in this study store 2500 mJ of energy. This energy is discharged by creating a short circuit between the anode and cathode of the battery using the armature, a piece of non-magnetic conductive wire. When this current moves through a magnetic field which is not parallel to the wire, a Lorentz force is induced, causing the wire to exert a force on the ground which is strong enough to propel the apparatus forward. By using various armatures and lubricants, top average speeds of 0.71 m/s were achieved. An electromechanical model of the homopolar motor is developed in PSpice. This simulation is used to predict the performance of the homopolar motor, including position and speed. Motor measured performance results and those predicted by computer simulation are compared and presented.

Nomenclature

a	Acceleration	Meter/Second^2
B	Magnetic Field Strength	Tesla
d	Displacement	Meter
F	Force	Newton
I	Current	Amps
k	Density	Kilogram/Meter^3
l	Length of Wire	Meter
m	Mass	Kilogram
q	Electric Charge	Coulomb
t	Time	Second
v	Velocity	Meter/Second
v_0	Initial Velocity	Meter/Second
v_f	Final Velocity	Meter/Second

Table of Contents

Contents

List of Figures

Figure

List of Tables

Table

Chapter 1 Introduction

The homopolar motor produces rotational movement from electromagnetism, making it the first electric motor. Michael Faraday created this device by extending a piece of wire into a pool of mercury with a magnet placed inside. When a current was supplied from a chemical battery, the wire would rotate around the magnet [2]. This motor was first demonstrated in 1831 by Michael Faraday at the Royal Institution in London. Since this device produced electromagnetic rotation, the homopolar motor helped create the foundation of modern electromagnetic technology [3].

The homopolar motor is a simple demonstration of the Lorentz force. When an electric current is not parallel to a magnetic field, a torque is induced known as the Lorentz force. This force is proportional to the cross-product of the electric field and the magnetic field. Therefore, the maximum force is induced when the two fields are perpendicular to each other. When the moving electric charges travel through a perpendicular magnetic field, the Lorentz force will induce a force orthogonal to both the current in the wire and the magnetic field. This force will cause the wire to rotate, therefore propelling the device forward.

The name 'homopolar' refers to the lack of polarity change. The magnets on either end of the motor are placed so that the polarity of each end is the same: either both north or south sides face outwards. Since the electric charge moves away from the battery at one end and enters the battery at the other end, the electric charge is moving in opposite directions on either end. Therefore, 'flipping' one of the magnets so only one polarity faces outward will allow both forces on the wire to act in the same direction. If the batteries were placed so that they had normal polarization (each end with different orientations – north facing outward on one end, south facing outward on the opposite end),

then the induced Lorentz force would contradict itself; one force would be directed upward on the wire while the force on the other end of the wire would be directed downward.

In the case of the homopolar motor, the main concept is to convert electrical energy into mechanical energy. The amount of mechanical energy produced is proportional to the amount of current involved, the strength of the magnetic field, and the length of the armature. Likewise, a homopolar generator converts mechanical energy into electrical energy. A conductive disk rotating in a magnetic field orthogonal to its axis will generate a voltage. The voltage will be proportional to the rotational velocity, strength of the field, and length of the conductor. Since the length between the axis and a point on the disk will help determine the amount of voltage generated, there will be a voltage potential difference between the center and outer edge of the disk. A sliding contact, or brush, on the circumference of the disk allows the electrical energy to be transferred to a load [10].

Despite its simplicity, or perhaps because of it, the homopolar motor still has relevance in today's technical society. It is used in a variety of modern-day applications, such as space launching, ship propulsion, and generating power for weapons and other devices. In addition to its simplicity, the homopolar motor provides many additional benefits, such as having a low cost of materials. It is also compact, and therefore appealing for use in weight- or area-sensitive applications. For example, it can be used as a direct electric drive for a ship [8]. In addition to ship propulsion, the homopolar generator can be used to power weapons or other equipment onboard a ship, allowing a large amount of power (in the MW-range) to be produced with little space required for the equipment [9]. Possible future applications may include replacing traditional turbine engines with an ultra lightweight machine for airborne applications [9].

Since the homopolar motor is still being adapted in new ways, this research intends to focus on modeling it to determine speed, rotational velocity, and position with variable inputs. An

electromechanical model of the motor is developed to predict its behavior over a period of time under a variety of conditions. The PSpice simulations are compared to the experimental test results to ensure accuracy.

The general outline of this thesis is divided into five sections. The first section includes the introduction and abstract. The second section develops the theory of the homopolar motor and includes the theoretical model in PSpice. The third section illustrates the physical experiment, including how the test is performed and what lubricants or armature shapes are used. The fourth section describes the experimental arrangement used to test the homopolar motor, including the general set-up and equipment used for testing procedures. Finally, the last section describes the results obtained at different levels to achieve the maximum speed from the homopolar motor.

Chapter 2 Theoretical Model

The theoretical model describes the electrical and mechanical characteristics of the homopolar motor. This section also describes the computer simulation, PSpice OrCAD, used to model the behavior of the homopolar motor.

2.1 Mechanical Theory

The homopolar motor is a simple and inexpensive mechanism or device which can propel itself forward using the torque provided by the Lorentz force. Below is a deconstructed homopolar motor. The main body of the device consists of a battery with two magnets on either end. For this experiment, rechargeable nickel-metal hydride (NiMH) batteries are used. The magnets used are 1/4" wide, grade N52 neodymium magnets purchased from an online distributer [1]. Washers are placed on both ends of the apparatus in order to reduce friction when the motor is being propelled forward. Finally, a copper wire creates the armature of the motor. In the picture below, a frayed copper wire is chosen in order to reduce contact friction by increasing the area of the contact and therefore reduce the overall resistance of the armature. This copper wire has to be routinely cleaned in order to remove any oxidation that may occur.

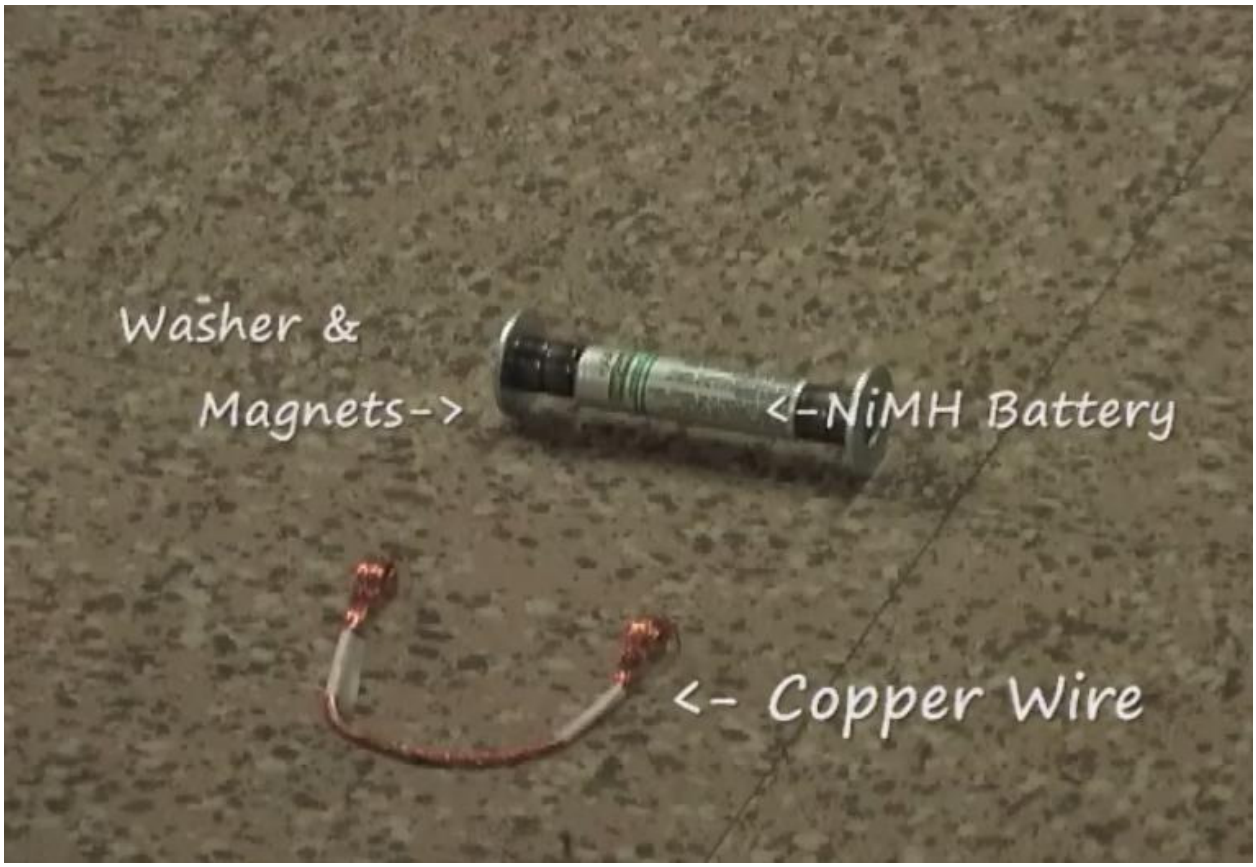

Figure 1.1: Deconstructed homopolar motor with frayed copper wire armature.

If an external magnetic field is applied perpendicular to the direction of current flow, the charged particles will experience a Lorentz force (see Figure 2.2). The Lorentz force is proportional to the cross product of the current and the magnetic field strength. Although the magnetic field and current do not necessarily have to be perpendicular, these two components are typically placed at right angles to each other in order to maximize the Lorentz force. In the equation:

$$F = q(v \, x \, B) \tag{1}$$

F is the net force (in Newtons), q is the electric charge of the particle (coulomb) moving with velocity v, and B is the magnetic field (tesla) [13]. Since the magnetic field is in the axial direction of the magnet and the current is in the radial direction since the charge flows along the surface of the magnet to the

wire, the direction of the force is perpendicular to both. Therefore, this equation can be simplified since the cross-product of two perpendicular entities will equal their product.

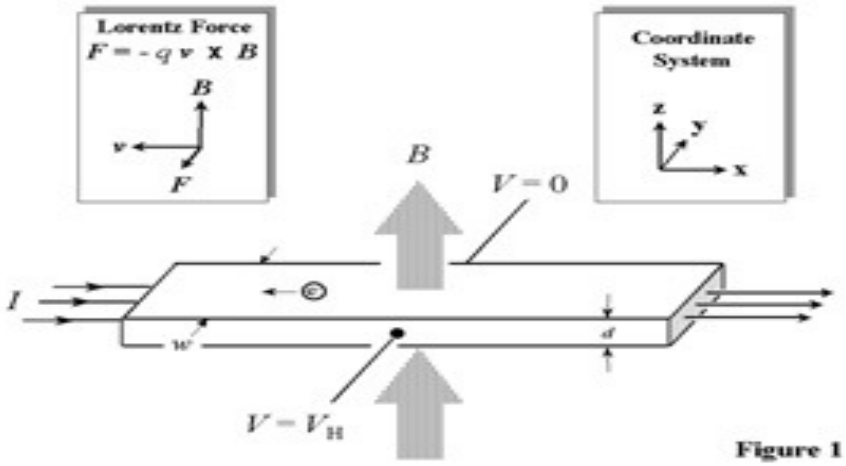

Figure 2.2: Lorentz force induced in a conductor placed in a magnetic field [6].

When the moving electric charge travels from one end of the battery to the other through the copper wire, it will cross the magnetic field. At the points along the electric loop where the direction of the wire is not parallel to the magnetic field, the Lorentz force is induced which is orthogonal to both [3]. This force produces a torque in the wire, forcing the wire to rotate and propel the entire apparatus forward.

2.2 PSpice Modeling

The homopolar motor was modeled using PSpice OrCAD 15.7. The equation for a force (F) applied to an armature can be calculated by multiplying the current (I), strength of the magnetic field (B), and length of the wire in the magnetic field (l) together [8]:

$$F = IBl \tag{2}$$

The calculated force can be used to find the acceleration, velocity, and position by using the following equations:

$$F = ma \tag{3}$$

$$d = v_0 t + \frac{1}{2} a t^2 \tag{4}$$

$$v_f = v_0 + at \tag{5}$$

where m is the total mass (in kilograms), a is the acceleration of the mass (meters/second^2), v_0 is the initial velocity (meters/second), v_f is the final velocity (meters/second), d is the displacement or position (meters), and t is the time (seconds) [11]. Since the velocity and position are the first and second order integrals of acceleration, respectively, the force and mass are the main parameters needed to describe the behavior of the motor. Once knowing these equations and the parameters of the system, the velocity and position can be calculated for any given time.

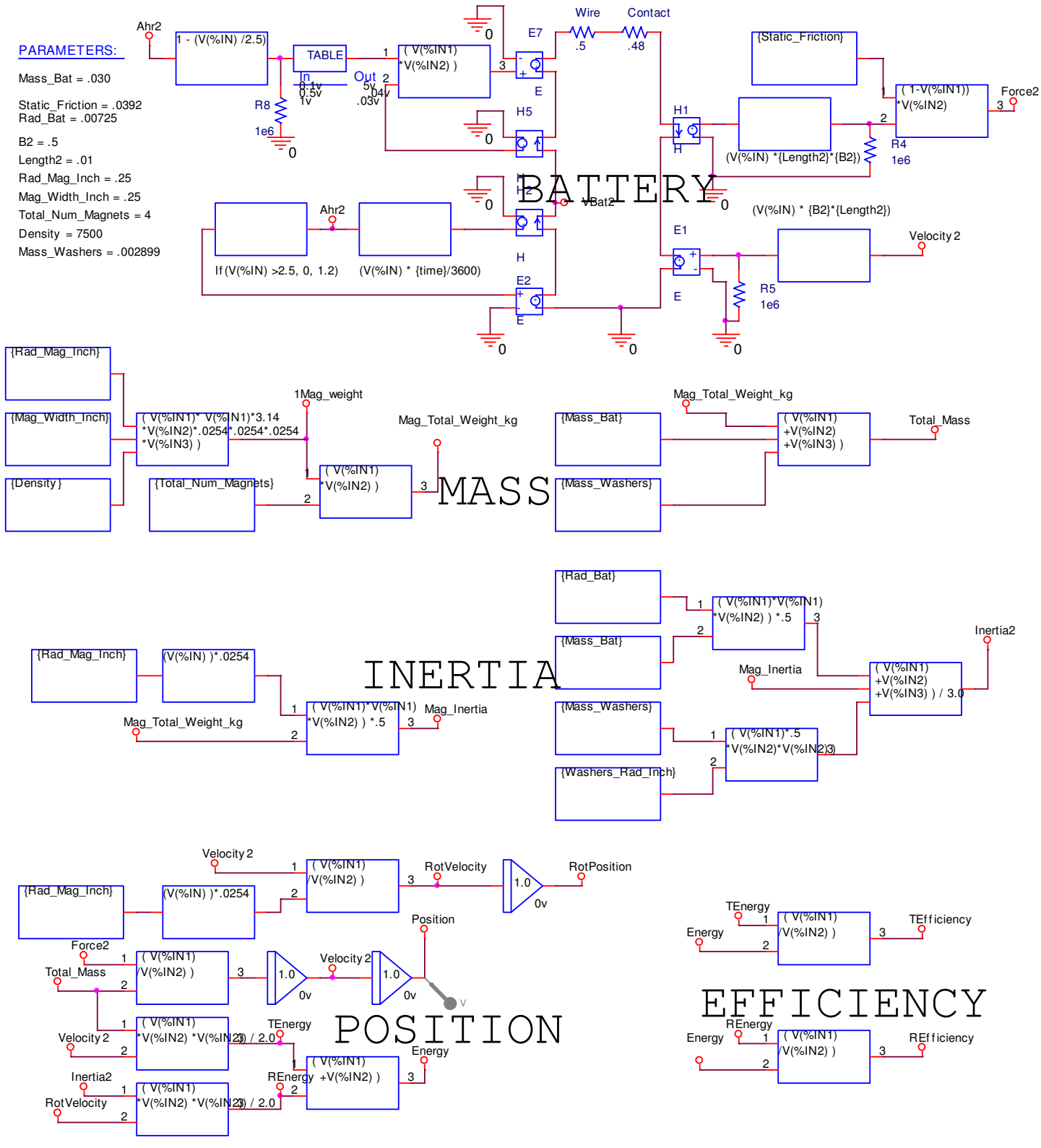

Figure 3.3: Complete PSpice simulation used to model a homopolar motor.

A PSpice simulation was created in order to simulate the mechanical model of the homopolar motor. Figure 2.3 represents the computer model used to find the position of the motor over an interval of time. This model is divided into five main sections: battery, mass, inertia, position, and efficiency. Various parameters were allowed to be changed, so the same simulation can be used with different batteries, magnets, and armatures. The known variables in this model are listed in the parameters table and can be changed if the tests are altered. This allows the fastest combination to be determined when using a parametric sweep.

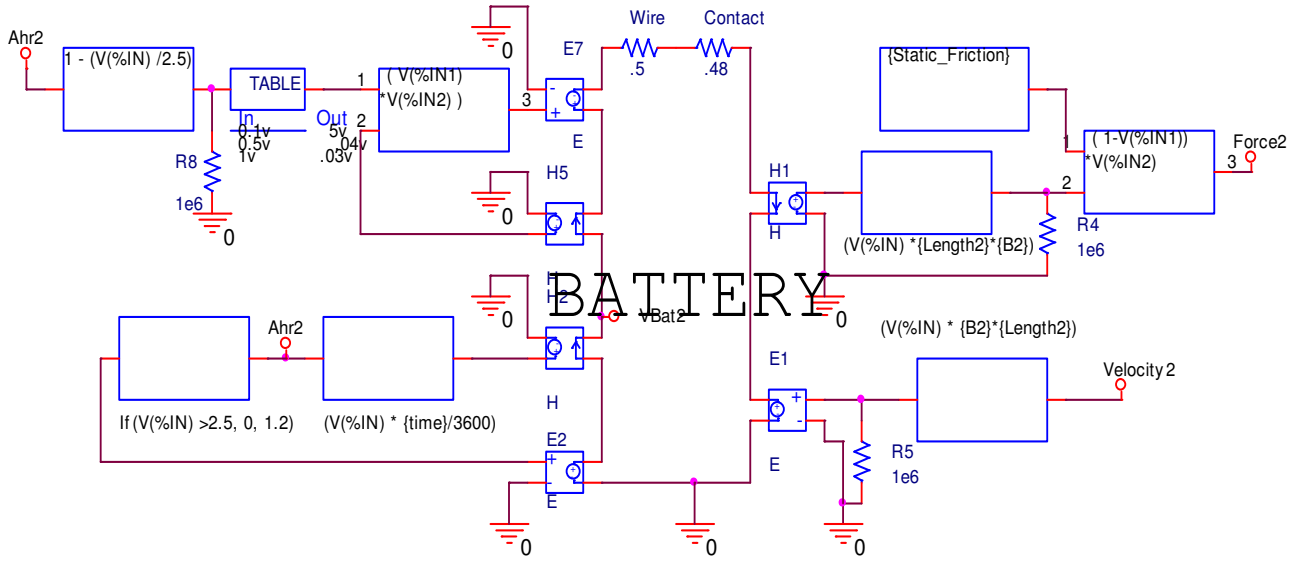

Figure 4.4: Modeling of battery power with discharge characteristics.

Figure 2.4 highlights the core area of the functioning model. It is divided into four sections which control the current in the model based on the rate and amount of time that the battery is being discharged. Figure 2.5 (below) depicts a current-controlled voltage-source that outputs into equation:

$$V(\%IN) * \{time\}/3600 \quad (6)$$

The voltage that the battery discharges multiplied by the time (given in seconds) gives the energy amp-seconds that the battery has discharged. Dividing by 3600 creates "Ahr2," or the number of amp-hours that the battery has discharged.

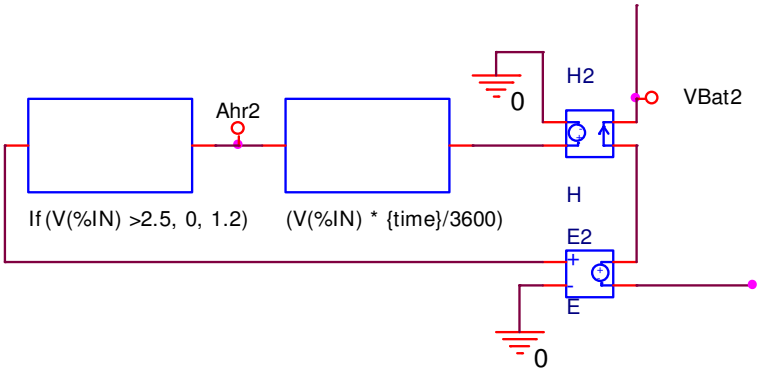

Figure 5.5: Calculation of amp-hours discharged to determine if energy is still available.

Since the battery is rated as 2.5 amp-hours, the ABM on the left determines if the battery has any energy left in it. If the battery has discharged 2.5 amp-hours or more, the output of the ABM is 0. This value feedbacks into the current-controlled voltage-source, turning it 'off' when the battery has fully discharged. When it still has energy available, the ABM will discharge 1.2 volts, or the rated nominal capacity of a nickel-metal hydride battery [4]. The amount of amp-hours discharged (Ahr2) that is calculated from this section is used to determine the internal resistance of the battery in Figure 2.6.

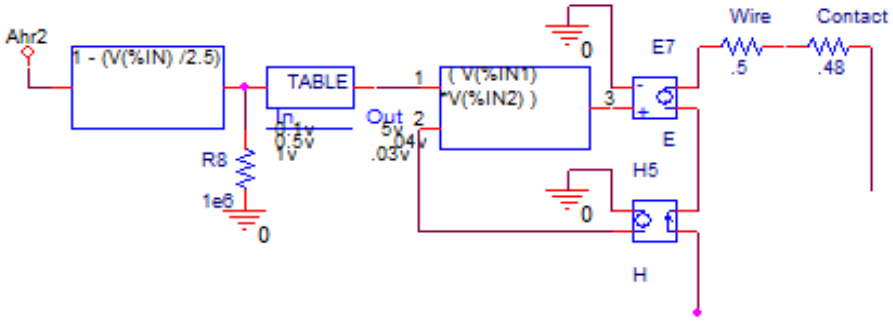

Figure 6.6: Internal resistance of the nickel-metal hydride battery based on energy still available.

The left side of Figure 2.6 has an ABM which outputs the percentage of the energy that is still available in the battery. The internal resistance of the battery changes depending on the amount of energy remaining in the battery. When fully charged, the internal resistance is 30 mΩ [4]. Likewise, a battery which is half-way discharged has an internal resistance of 40 mΩ [4]. When very little energy is left, the internal resistance is very high. An estimation of 5 Ω is used for when very little energy remains (10% or less). This is significantly higher than the previous internal resistance, so in comparison, the resistance is over two orders of magnitude larger. A table is used to determine the internal resistance based on the amount of battery power still available in the battery.

The table feeds into an ABM which multiplies the internal resistance with one of two values depending on if power is still available in the battery. When it has been fully discharged, H5 will have a 0 amp input, so V(%IN2) will also be zero. A voltage source will output a voltage proportional to the product of the internal resistance and battery voltage.

In addition to the internal resistance, Figure 2.6 also includes the wire and contact resistance. The wire resistance is the measured resistance of the armature. The contact resistance had to be altered depending on the type of armature and lubricant used. For the frayed copper armature without any lubrication, the wire resistance is 0.5 Ω and the contact resistance is 0.75 Ω.

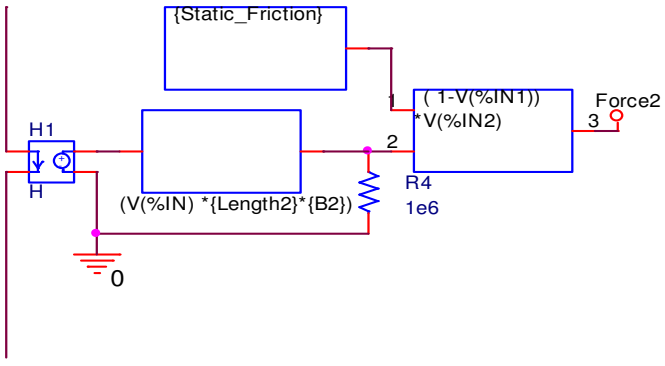

Figure 7.7: Force induced on an armature based on current and magnetic field strength.

Figure 2.7 depicts a current-controlled voltage source which is used to calculate the force acting on the armature. The force is proportional to the strength of the magnetic field (B2), the current (V(%IN)), and the length of the wire on which the force is induced (Length2). Since it is assumed that the magnetic field is perpendicular to the wire and therefore the current, the force on each piece of wire is 0.5*I*B*L. Since the force is on two ends of the wire, the combined force on the wire is I*B*L.

The static friction is 0.0392. This is experimentally found by placing the apparatus on a board of known length and raising one end of it until the device begins to roll. The height is measured at the point where the movement begins, which allows the angle and the coefficient of static friction to be calculated. After subtracting the friction acting on the motor, the total force used to propel the apparatus is Force2, or 96.08% of the total force.

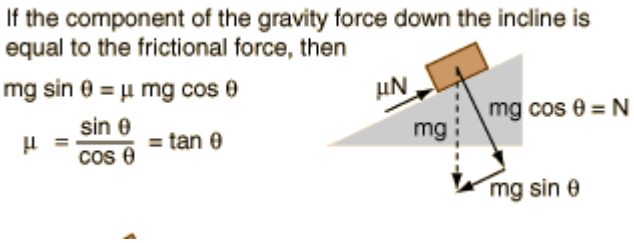

Figure 8.8: Finding the static friction of an object using an inclined plane [5].

Finally, the fourth section is used to calculate the back voltage. The back voltage is generated when the armature moves through the magnetic field. It is calculated in the ABM in Figure 2.9 by multiplying the velocity with the magnetic field and length of the wire. This value goes into a voltage-controlled voltage source, causing a reduction in the 1.2 nominal voltage used in the previous sections.

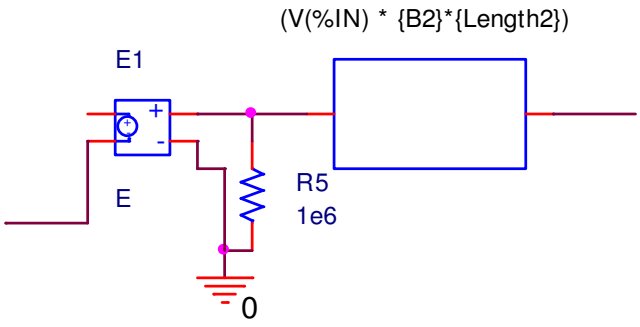

Figure 9.9: Back voltage generated from the armature traveling through a magnetic field.

Next, we will look at calculating different parameters with varying inputs. Figure 2.10 calculates the total weight of the magnets to be used in the homopolar motor. Given the radius and width of a magnet, the volume of the magnet can be calculated in meters cubed. Once this value is found, it is multiplied by the density of the magnet in order to find the total weight. For the type of magnet chosen, the density is 7500 kg/m^3. This number is determined by using the given mass of 6.03 grams for a magnet with a radius and width of 0.635 cm [1]:

$$6.03grams = k * V = k(\pi r^2 w) \tag{7}$$

$$6.03grams = k * 3.14 * 0.635\ cm^2 * 0.635\ cm$$

$$k = 7{,}500{,}000\ g/cm^3 = 7500\ kg/m^3$$

Therefore, the weight of any neodymium magnet can be found as long as the radius and width are known. Since the dimensions on kjmagnetics.com are given in inches, the width and radius is inserted into the parameters table in inches. The ABM3 block converts the units into meters as it multiplies the volume with the density, therefore finding the weight of one magnet. Finally, to find the total weight of the magnets, the mass of one magnet is multiplied by the total number of magnets. To control this part of the simulation, the radius of the magnet (in inches), width of the magnet (in inches), and the total number of magnets used can be changed in the parameters table under the names Rad_Mag_Inch,

Mag_Width_Inch, and Total_Num_Magnets, respectively. Also, if a magnet is used that does not have a body of NdFeB material, the density (in kg/m^3) can be changed in the parameters table.

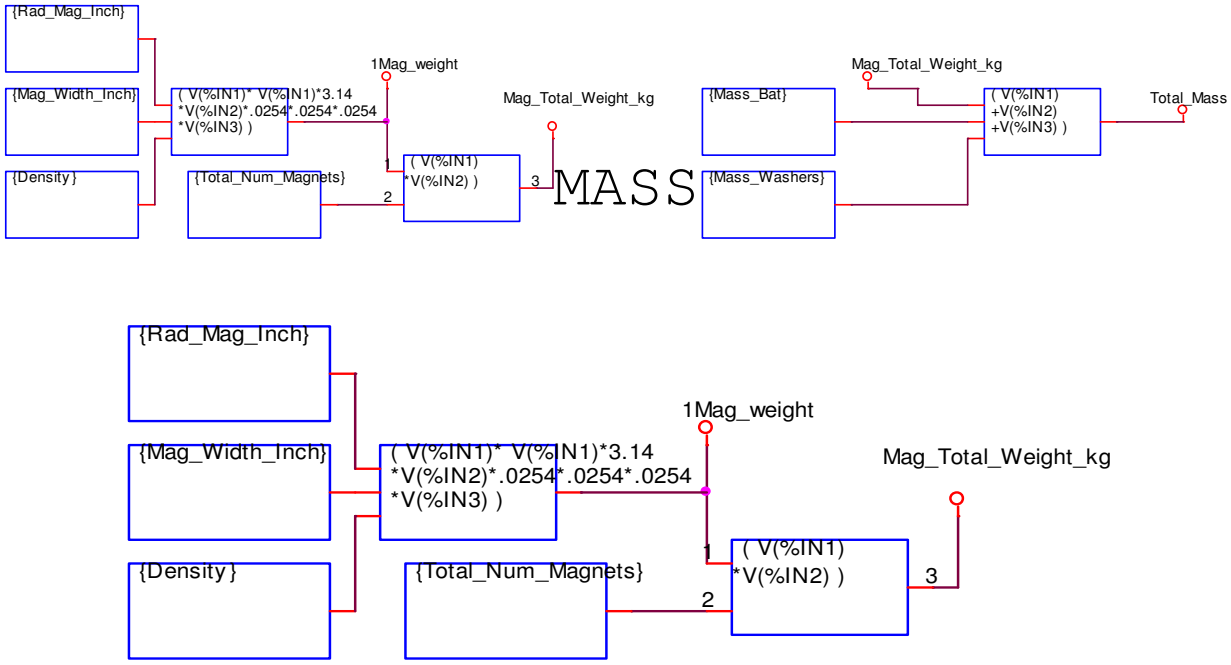

Figure 10.10: Calculation of total magnet mass given the magnet's dimensions.

The total mass of the motor is calculated in Figure 2.11. It is found by adding the total weight of the magnets (see Figure 2.10) with the weight of the battery and washers. The battery and washer weight is input by the user into the parameter table under the labels Mass_Bat and Mass_Washers. The battery mass given is found on the Energizer product data sheet and the washers are weighed.

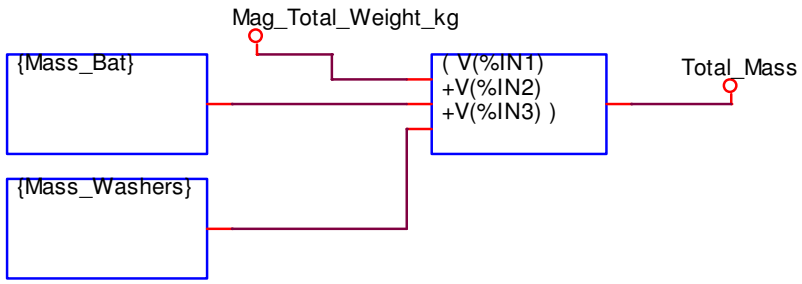

Figure 11.11: Total mass of the homopolar motor.

Likewise, Figure 2.12 shows the inertia calculation of the magnet. The inertia of a magnet is calculated by multiplying the weight (in kg) by the square of the radius of the magnet (in meters). Since the radius of the magnet is input in inches, the units have to be changed into meters by multiplying by .0254 m/inch. The moment of inertia of a solid cylinder or disc is:

$$I = \frac{1}{2}MR^2 \tag{8}$$

This equation is used to find the moment of inertia of the body of the motor, including both the magnets and the battery (see Figure 2.13).

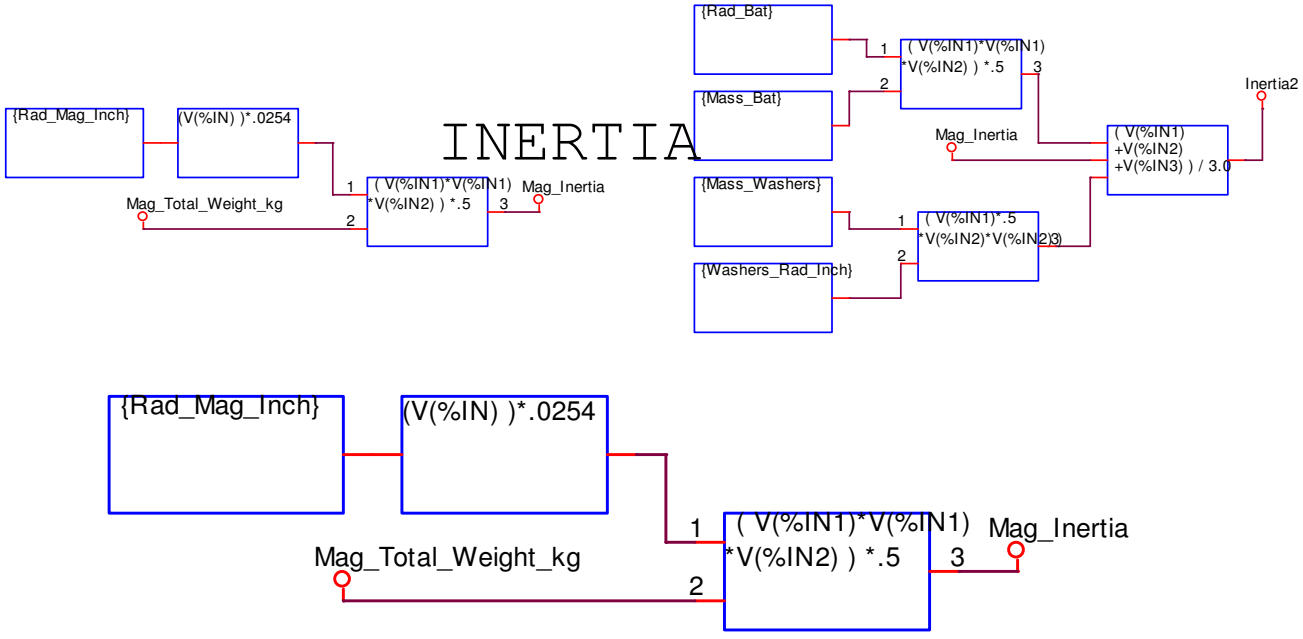

Figure 12.12: Inertia section including the calculation of the inertia of the magnets.

The magnet inertia is used to find the total inertia of the apparatus. The inertia of the battery and washers are also calculated in this section. The inertia of a solid cylinder is $I = 0.5MR^2$, where R is the radius of the battery and M is the mass of the battery in meters and kg, respectively [7]. These values are measured and placed in the parameters sections located in the top left corner. Therefore, if

an alternative battery is used, the simulation will still be applicable after changing these two values. The total inertia is found by summing the battery, washer and magnet inertias together.

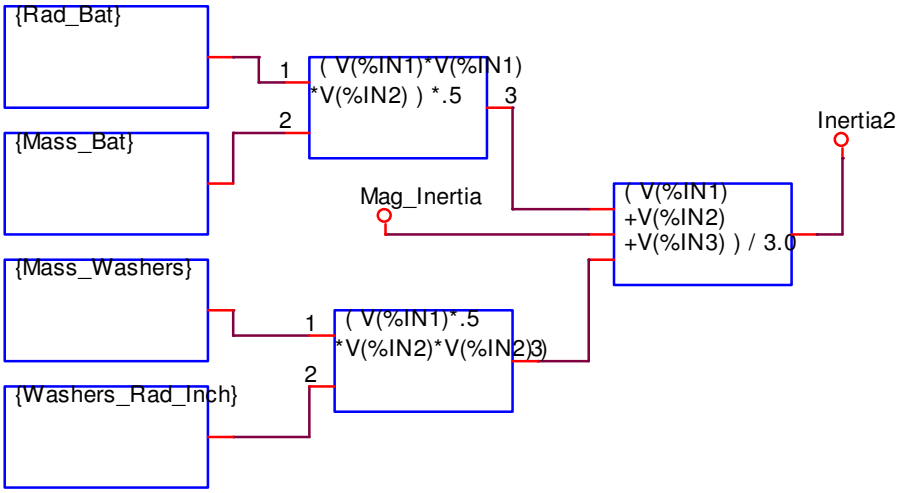

Figure 13.13: Total inertia of the system found by summing the battery, magnet, and washer inertias.

Figure 2.14 highlights the section of the PSpice simulation which calculates the position, velocity, and energy of the motor. This part of the model consists of four ABM blocks and two integrators. Using Newton's second law of motion, the acceleration of an object (a) can be found if the force (F) and mass (m) of the object is known:

$$F = ma \tag{3}$$

$$a = F/m$$

In the above equation, the units of force, mass, and acceleration are given in Newtons, kilograms, and m/sec^2, respectively. The integral of the acceleration gives the velocity, and the integral of the velocity is the position. The position can therefore be plotted over an interval of time. This graph will be displayed in the results section.

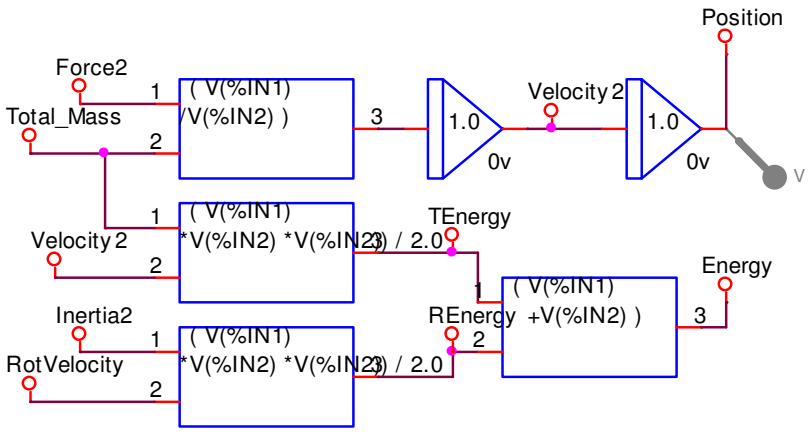

Figure 14.14: Position and energy of the system calculated from the force, mass, and inertia found in previous sections.

The energy of the device can be determined by calculating the translational and rotational energy. The translational energy is half the total mass multiplied by the square of the velocity:

$$Linear\ KE = \frac{1}{2}mv^2 \tag{9}$$

Similarly, the rotational energy is half the inertia multiplied by the square of the rotational velocity [8]:

$$Angular\ KE = \frac{1}{2}I\omega^2 \tag{10}$$

The total energy is the sum of the translational and angular kinetic energies.

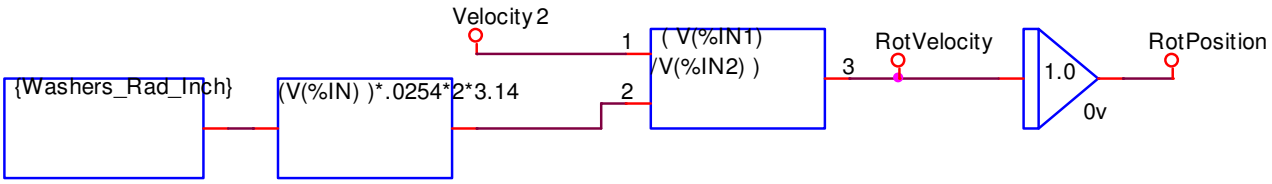

Figure 15.15: Rotational velocity calculated from the translational velocity and apparatus circumference.

There is a direct relationship between the laws of motion for linear and angular motion. Therefore, the rotational position is found by taking the integral of the rotational velocity like the linear

position was found previously using the linear velocity. The rotational velocity is calculated by dividing the positional velocity by the circumference of the washers (in meters).

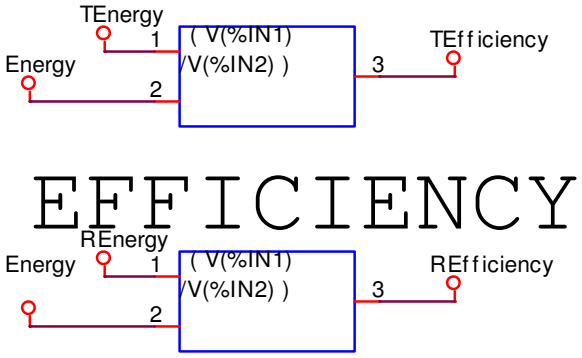

Figure 16.16: Translational and rotational efficiency of the system.

Finally, the efficiency was calculated for both the translational and rotational energy. For maximum speed, we want the translational efficiency to be as large as possible.

Chapter 3 Experimental Devices

The experimental devices used for testing the homopolar motor include a rechargeable battery, neodymium magnets, two washers, a nonmagnetic conductive wire, and a ten-meter long track. Additionally, a video camera is used to record the experiment. The data gathered from this video are processed to find the velocity and position of the apparatus at one-meter intervals along the racetrack. Each of these items will be discussed below, including the purpose and physical parameters of each element.

3.1 General Overview

Experiments were conducted to compare the accuracy of the PSPICE simulation with physical results across a distance of ten meters. For these tests, homopolar motors are constructed using one of four available nickel-metal hydride batteries, each to be used a total of three times during the course of testing a new armature or lubricant. The batteries are to be fully charged prior to each new run. These physical experiments are divided into one of two groups based on lubrication or armature material. Although experiments in both groups are conducted using a battery, washers, and magnets, the contact resistance will be different because of the chosen lubricant or material of the armature.

3.2 Battery

The type of battery selected is the Energizer NH15-2500. This rechargeable battery has a nickel-metal hydride (NiMH) chemical system. It has a nominal voltage of 1.2 volts and a rated capacity of 2500 mAh at room temperature (70° F) based on a 500 mA continuous discharge rate to 1.0 volts. The battery has an internal resistance 30 mΩ when fully charged and 40 mΩ when the cell is half-way discharged [4].

The physical dimensions of the NiMH battery according to the Energizer product datasheet is a diameter of 14.5 mm, length of 50.5 mm, and weight of 30 grams [4]. Although the typical weight given

on the parameters sheet is 30 grams, the actual measured weights of the batteries are slightly lighter. Each weight is listed in Table 3.1.

Table 3.1 – Measured battery weight

Battery 1	28.83 grams
Battery 2	28.67 grams
Battery 3	28.63 grams
Battery 4	28.84 grams

The type of battery selected is the nickel-metal hydride battery because it gives a more consistent current while it discharges versus alkaline and lithium-based batteries. Figure 3.2 below shows the discharge rate for the Energizer battery which is chosen.

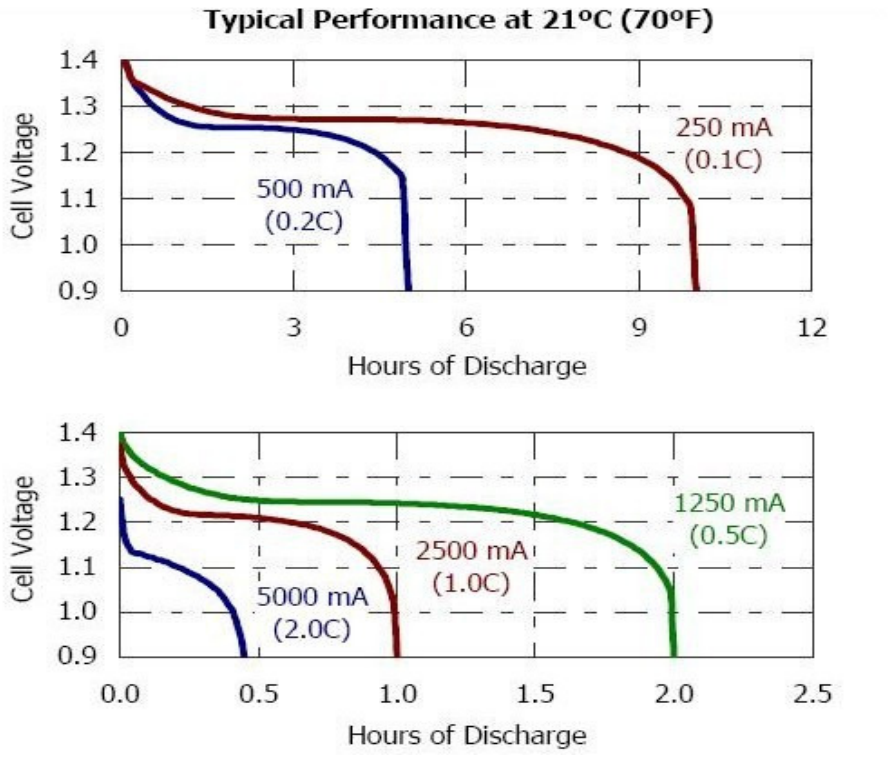

Figure 3.2: Energizer nickel-metal hydride battery discharge curves [4].

3.3 Magnets

The magnets are acquired from an online company, www.kjmagnetics.com. For the purpose of this thesis, the same four magnets are used in every experiment. These magnets are grade N52 neodymium magnets with 1/2'' diameter and 1/4'' width. These neodymium magnets consist of a NdFeB body coated with a nickel plating weighing 6.03 grams each. The actual measured total weight of two magnets and one washer is 26.77 grams and 26.34 grams for each respective side.

Neodymium magnets are chosen because they are strong and have a nickel coating. The nickel coating (as opposed to a standard ceramic magnet) is necessary because it conducts electricity and allows the wire to slide easily along the surface [12]. The N52 magnets are the highest available grade magnets available from this manufacturer. The diameter of the magnet is chosen to be slightly larger than the diameter of the battery. This allows a large enough space for the brush to maintain contact with the circumference of the magnet while avoiding the larger moment of inertia caused from a larger diameter magnet.

The magnetic field of the homopolar motor can be seen in Figure 3.3. Since the battery is metallic, the magnetic field can travel through the battery as well as around the outside of the battery. This field was experimentally measured using a teslameter. The magnetic field strength is proportional to the distance of the magnet. For the purpose of this research, the magnetic field is measured half-way between the magnet and the point of contact on the floor of the armature. This value is inserted into the parameter's table of the PSpice simulation.

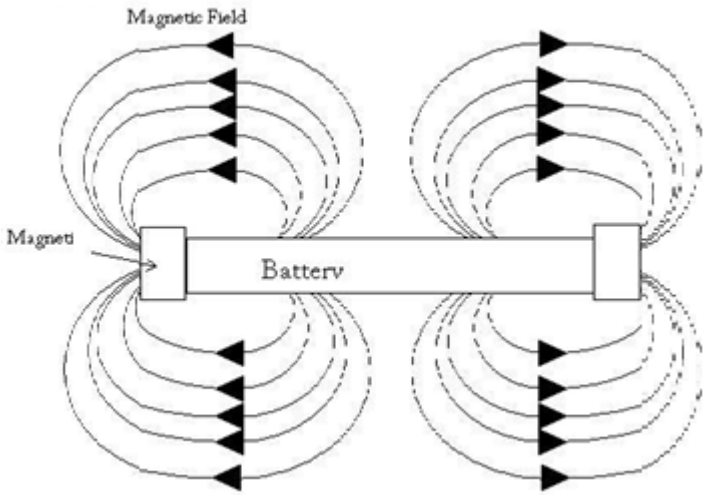

Figure 3.3: Magnetic field of a homopolar motor. The magnetic field extends into the battery because of its metallic casing.

3.4 Washers

The washers are added to the ends of both magnets in order to reduce contact friction. The magnets hold the washers in place, and since the washers have a larger diameter than the magnets and battery, contact resistance is reduced because the magnets and battery do not touch the track.

3.5 Armature

A nonmagnetic, conductive wire is used as the armature. This armature makes contact with the circumference of both magnets, connecting the anode and cathode end of the battery together through the magnets and wire. For the lubricant section, the armature is composed of a frayed copper wire which is dipped in a variety of liquids. The alternate group of experiments consists of armatures of different material, including nickel-plated copper and solder.

3.6 Track

A ten-meter track has been constructed on a flat tiled surface located in the east hallway on the second floor of Engineering Building West. The track is marked at one-meter intervals using transparent tape colored with a red marker. These markers were used to help determine the velocity of the homopolar motor in conjunction with the video camera.

Chapter 4 Physical Experiment

Experiments are conducted to compare the accuracy of the PSPICE simulation with physical results. A ten-meter track has been constructed on a flat tiled surface. Four homopolar motors consisting of a single nickel-metal hydride battery and a conductive wire are used to conduct each test.

Four nickel-metal hydride batteries are used in total, each to be used a total of three times during the course of testing a new armature or lubricant. These batteries are fully charged prior to each experiment and are fully recharged prior to both the second and third trials for each new armature and lubricant.

The physical experiments can be subdivided into two groups based on if the focus of the experiment is testing a lubricant or an armature. The first group of experiments is conducted using a dry, frayed copper wire, a rechargeable nickel-metal hydride battery, two neodymium magnets, and two washers in addition to a lubricant. The second group is also conducted using the battery, washers, and magnets, but armatures of different material are used in place of the frayed copper wire.

Three tests are conducted in total for each lubricant or type of armature. The second test has the apparatus running from the zero- to ten-meter mark on the track. Likewise, the third test consists of the device traversing from the ten- to zero-meter mark for all four batteries. The first test has the direction of travel alternating between each battery. Therefore, any slope or variations of the level of the track will be accounted for by averaging the results.

4.1 Lubricants

As an initial test, the homopolar motor is propelled using a dry armature composed of a frayed copper wire. Experiments are then conducted using the same frayed copper wire with a variety of lubricants: tap water, salt water, soapy water, and mineral oil. Since copper will oxidize when exposed

to air, the copper armature is cleaned for each experiment prior to using a freshly charged battery. A 5% hydrochloric acid (HCl) solution is applied to the contacts of the wire using a q-tip applicator. This applicator is used to lightly scrape the leads of the armature in order to remove any oxidation residue. Next, the solution is rinsed off using tap water and the armature is blotted dry. The 5% HCl solution is used for the experiments involving tap, salt, and soapy water in addition to mineral oil as a lubricant. Due to a shortage of the original HCl solution, a stronger solution has to be substituted for subsequent experiments. Therefore, the 'dry' experiment which has no lubricant applied to the armature is conducted using a 37% HCl solution as the cleaning agent on the oxidized copper. The oxidization on the frayed copper leads can be seen in Figure 4.1.

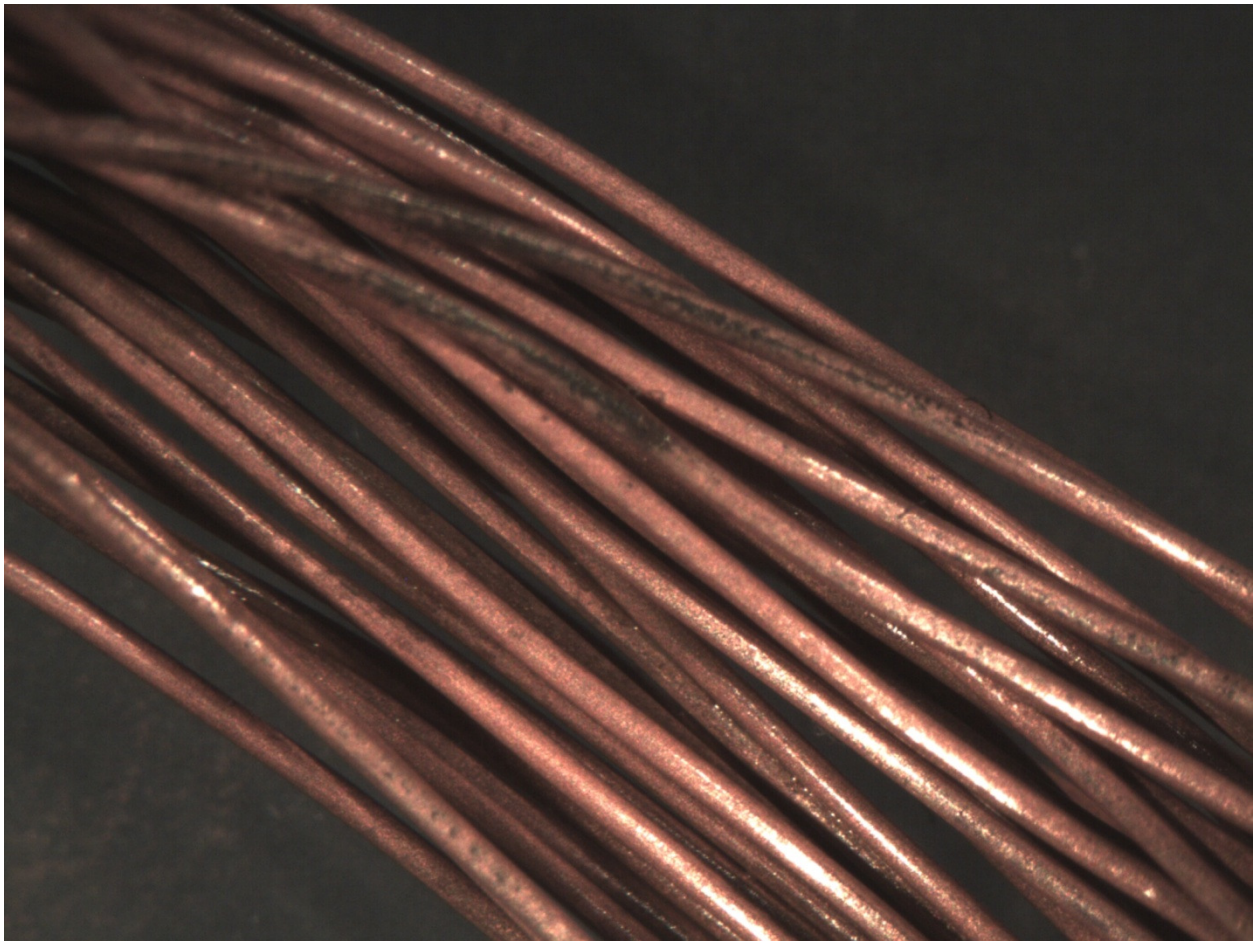

Figure 4.1: Oxidation on the frayed copper wire armature.

After the HCl solution is used to clean the frayed copper wire, the ends of the armature are dipped into a lubricant. Each lubricant is placed in a container so it can be reused for each fresh battery in the experiment. This will encourage uniformity between each test. The containers can be viewed in Figure 4.2. The salt-water solution is created by slowly stirring salt into a container of water until the solution becomes saturated. Likewise, dish soap is added to a container of water. Since it is difficult to determine when the liquid soap will saturate the water, the soap-water mixture is created by combining an equal amount of soap and water. The mineral oil lubricant is not diluted like the other lubricants.

Figure 4.2: Containers holding each of the four lubricants.

4.2 Armature Modifications

Next, different materials and shapes are used to vary the armature. Since the lubricants do not excessively speed up the device, armature modifications are tested to try to maximize the velocity of the homopolar motor. In these experiments, each wire is dry and no lubricant is applied to the armature or

body of the device. If copper wire is to be used, the oxidation is cleaned off of it using a 37% HCl solution and tap water. This will be blotted dry before the experiment is subsequently conducted.

The first experiment using a different form of armature consists of a frayed copper wire similar to the previous copper armatures but with an additional loop (see Figure 4.3). This shape uses the loop in hopes of doubling the current through the magnetic path, therefore ensuring twice the Lorentz force acting on the device. Therefore, the same amount of current and magnetic field strength could produce a faster speed. This experiment was not successful, however, and will be discussed in more detail in the results section.

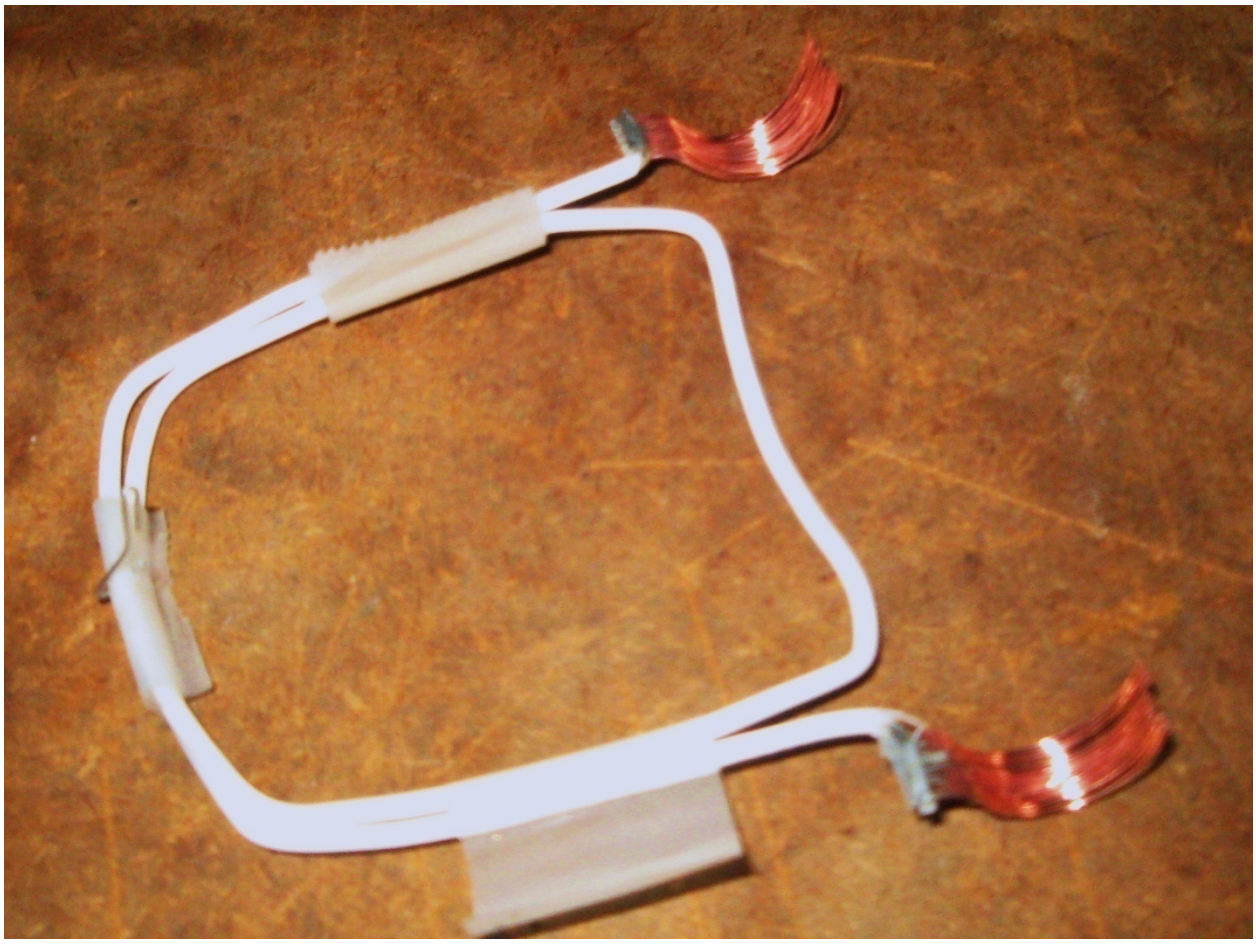

Figure 4.3: Double-turn armature used to double the current in the Lorentz force calculation.

Nickel-plated copper wire is also used to construct an armature. The material used is a piece of copper flat braid with ¼" width with a thin layer of nickel over it. Although nickel has a higher resistance than copper, it does have the advantage of resisting oxidization. Therefore, the HCl solution is not necessary to clean the armature before testing. Since the nickel plating is thin, it is hoped that the additional resistance would not have a large impact on the overall armature resistance. However, since the resistivity of copper over that length is significantly low, the nickel added a large resistivity to it proportionally.

Finally, a single strand of solder is used for the armature material. The first type of solder was not successful for this application. When testing the homopolar motor using the solder armature, the first experiment was conducted with Battery #1 and a 0.031 inch diameter solder with standard rosin core consisting of lead and tin. This first test was inconclusive. The motor seemed to travel fast for the first few meters, but slowed quickly after that, barely completing the 10 meter run. When the motor was retrieved, the armature was found to be broken (see Figure 4.4 below). Since the melting temperature of solder is low (approximately 373° F), the heat caused from conducting a large amount of current in combination with the Lorentz force caused the armature to break [14].

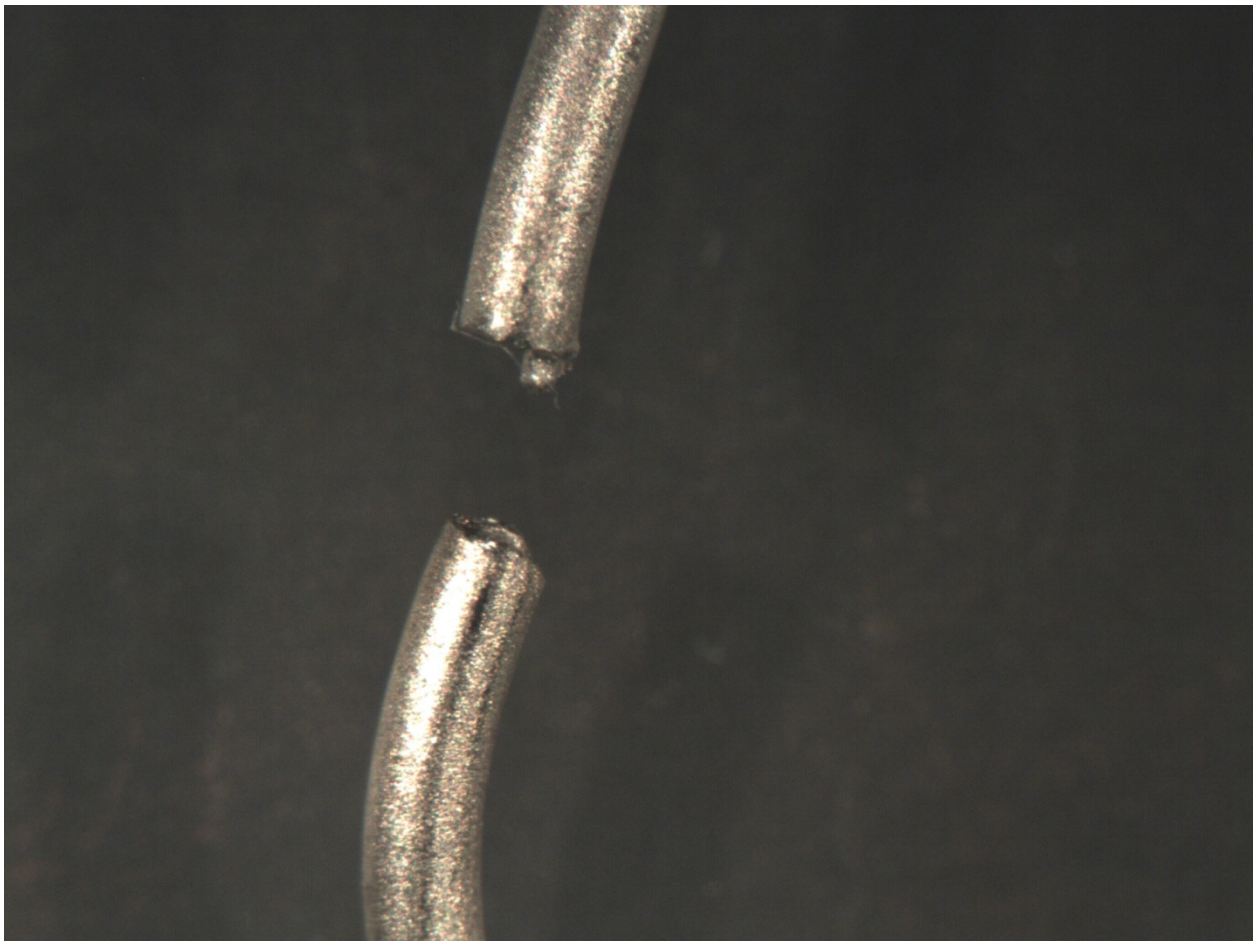

Figure 4.4: Solder armature break-point with a 0.031 inch diameter.

In order to overcome this setback, a larger diameter solder is used. Next, 0.062-inch solder with standard rosin core is shaped to form the armature. The trials from this new wire are exceptional compared to previous experiments. Battery #2 is able to complete the full 10 m racetrack in 10.8 seconds. Therefore, the solder seems like a viable material for an armature, and the subsequent 12 experiments are conducted and recorded.

Chapter 5 Results

A total of 12 test runs are conducted with each new type of lubricant or armature material. These trial runs consisted of six motors running the track from the beginning or zero-meter mark to the end or 10-meter mark and six traveling in the opposite direction. This will compensate for any irregularity or slope on the chosen track site. The first five experiments focus on lubrications for the armature. In addition to a non-lubricated or 'dry' experiment, the armature is dipped in tap water, salt water, soapy water, and mineral oil. By controlling the shape of the armature, the lubricant applied to it, and the material of the armature, one can tailor the force to a range of magnitudes.

Experiments are conducted to compare the accuracy of the PSPICE simulation with physical results. A ten-meter track is constructed on a flat tiled surface. Four homopolar motors consisting of a single nickel-metal hydride battery and a conductive wire are used to conduct each test. Three tests are conducted for each lubricant or type of armature using all four batteries. The second test has the apparatus running from the zero- to ten-meter mark on the track. Likewise, the third test consists of the apparatus traversing from the ten-meter to zero-meter mark for all four batteries. The first test has the direction of travel alternating between each battery. Therefore, any slope or variations of the level of the track will be accounted for by averaging the results. The experiments had overall averages of 14.9 seconds for the first group of tests (alternating directions), 16.3 seconds for the second group (heading towards the ten-meter mark), and 15.0 seconds for the third group of tests (heading away from the ten-meter mark). Therefore, the aperture performed 8.7% faster for traveling from the ten-meter mark to the zero-mark versus the same armature traversing in the opposite direction.

The average resulting time for each lubricant is presented in table 5.1 below. Since these are within 5.4% of their average and they have a standard deviation of 2.68, the lubricants are not determined to produce significantly different results.

Table 5.1: Lubricant average times

LUBRICANT	AVERAGE TIME	STANDARD DEVIATION
DRY	15.63	2.66
TAP WATER	15.57	2.61
SALT WATER	15.73	2.68
SOAPY WATER	16.85	3.50
MINERAL OIL	16.18	1.96

These results are consistent with the PSpice simulation. Figure 5.2 shows the position of the homopolar motor with respect to time. Note that the estimated time to complete a 10-meter track is 16 seconds, which is close to the average measured time of a homopolar motor with a frayed copper armature.

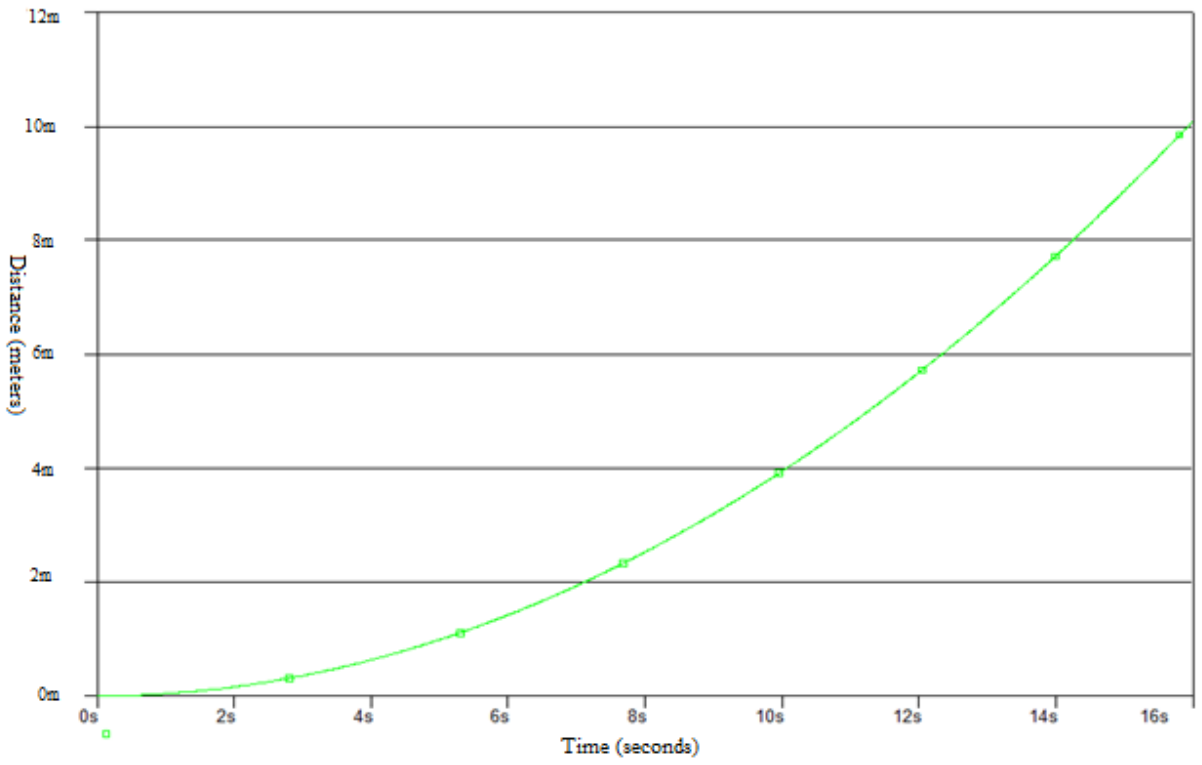

Figure 5.2: Time vs. position PSpice simulation results.

Tables 5.3 and 5.4 display the simulated and actual results for time vs. position over a ten-meter interval. The physical results section is the average times for the dry experiments. Although the physical tests accelerate faster than expected, the simulated and actual results became more correlated as the time became larger. At 10-meters, the difference in times is only 2.4%.

Table 5.3: Simulation results for a dry copper armature homopolar motor.

Distance (m)	1	2	3	4	5	6	7	8	9	10
Time (s)	5.10	7.00	8.70	10.0	11.25	12.30	13.25	14.25	15.10	16.00

Table 5.4: Physical results for a dry copper armature homopolar motor.

Distance (m)	1	2	3	4	5	6	7	8	9	10
Time (s)	3.99	5.73	7.22	8.57	9.83	11.07	12.23	13.35	14.47	15.63

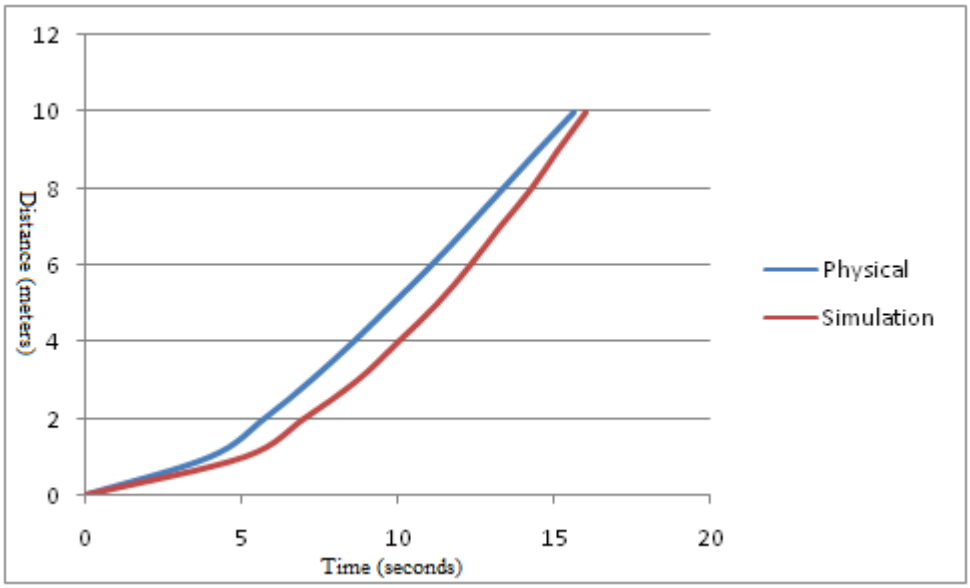

Figure 5.5: Time vs. distance graphs for the simulated and physical results using a dry copper armature.

Different materials and shapes are also used to vary the armature. Since the copper wire with an applied lubricant does not seem to have much advantage over using a dry armature, armature modifications are tested without lubrication to try to maximize the velocity of the homopolar motor.

The average times of the experiments using the armatures modified with different types of material are listed in the table below. These produced significantly different results with a standard deviation of 6.4 between the three armature types.

Table 5.6: Armature material and shape average times

MATERIAL	AVERAGE TIME	STANDARD DEVIATION
DOUBLE-TURN ARMATURE	25.97	3.97
NICKEL-PLATED ARMATURE	21.68	4.76
SOLDER ARMATURE	14.07	1.32

There is a significant improvement when solder is used as the material of the armature. Even dry frayed-copper wire is less effective than the solder armature since the average times ranged from 15.57 seconds to 16.85 seconds. This is a 10% improvement over the next fastest time. Additionally, the solder model is more efficient than the copper model. Although the solder model uses 800 mJ as compared to 640 mJ for the duration of the time to transverse 10 meters, the solder model is more efficient since a larger percentage of the energy is dedicated to translational energy. The solder and copper models use 7.04% and 6.83% of their energy for translational motion, respectively.

The first experiment using a different form of armature has not been successful. The double-turn armature consisting of a frayed copper wire similar to the previous copper armatures is constructed but with an additional loop. This shape is used in hopes of doubling the current through the magnetic path. Although approximately the same amount of current is running through the armature, this current will go through the magnetic path twice as much, hence ensuring twice the Lorentz force acting

on the apparatus. Therefore, the same amount of current and magnetic field strength will produce a faster speed. Although the current involved will not be fully doubled since resistance from the additional length must be accounted for, it will still be much larger. The added resistance of the wire will lower the amount of current in each wire path, but since the contact resistance is much larger than the resistance from the length of wire, the additional current paths will still produce a net current larger than the original individual current path.

Unfortunately the experiments prove this new construction is less efficient. The times are much slower, varying from 21.8 to 34.3 seconds with an average time of 26 seconds in order to complete the ten-meter run. This is because forces act on the additional section which runs parallel and close to the battery, causing the wire to bend. The misshaped wire is twisted so that one side is forced down, causing the motor to veer sideways. Additionally, the armature is not able to maintain its original contact since the twisted wire only lets some of the frayed ends lie on the magnet. This causes a larger contact resistance, and therefore a smaller current to conduct through the armature.

A nickel-plated copper wire is used to construct the next armature. The nickel plating is thin, so the added resistivity should not have a large impact on the results. However, since the resistivity of copper over that length is significantly low, the nickel added a large resistivity to it proportionally. The times for this set of experiments were much slower, ranging from 15.8 to 32.8, with an average time of 21.7 seconds.

In experiment 1 while using solder as the armature, each battery is able to finish between 11.7 and 12.2 seconds. In the initial trial run, however, the .062 solder and battery are able to finish at 10.8 seconds. This is partially due to the placement of the wire. The brush is applied to the magnets for a moment before the armature is released and able to make contact with the floor. This allows for a Lorentz force to be induced before the armature touches the ground.

Since it was not fully released when the armature made initial contact with the magnet, the Lorentz force caused the battery to begin rolling forward since the wire was stationary. Therefore, this caused the time to be recorded as only 10.8 for the 10 meter run, which is a full second lower than subsequent tests.

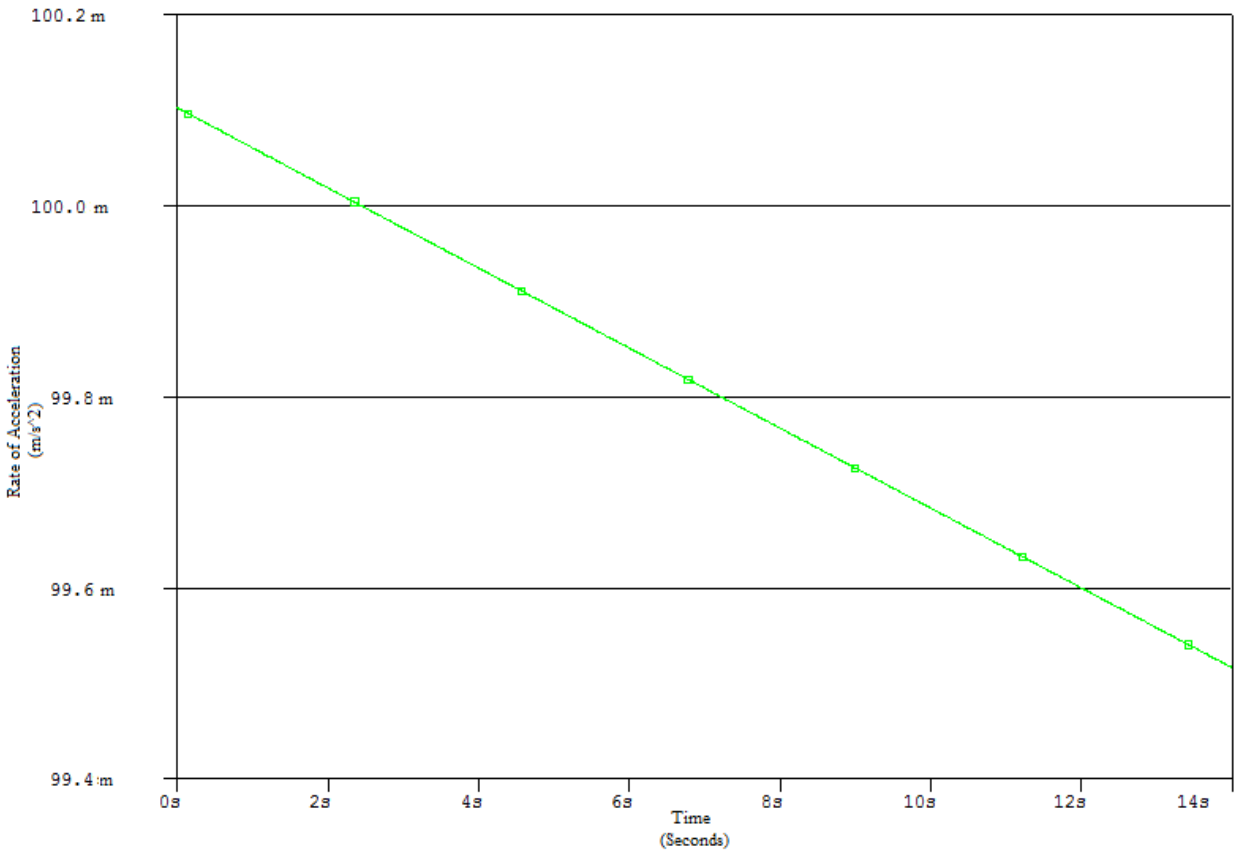

Figure 5.7: Time vs. rate of acceleration for the solder armature model.

The solder armature produces faster results than all previous experiments. As expected, the apparatus obtains maximum velocity at the beginning of its run and the rate of acceleration decreases as the battery discharges. See Table 5.7 for a complete list of clocked times for each position. The graph displayed in Figure 5.8 shows the solder armature has a quicker time for every position, producing results equal to or exceeding 10% faster than all other experiments performed.

Table 5.8: Time (in seconds) for each meter interval distance (in meters)

Distance (meters)	Dry	Tap	Salt	Soap	Mineral	Nickel	Double	Solder
				Time	(seconds)			
1	3.99	4.56	4.25	4.05	4.15	4.34	5.75	3.27
2	5.73	6.41	6.10	5.85	5.96	6.43	8.26	4.74
3	7.22	7.88	7.60	7.48	7.50	8.43	10.50	6.05
4	8.57	9.13	8.95	8.96	8.93	10.30	12.65	7.30
5	9.83	10.34	10.20	10.39	10.27	12.13	14.78	8.49
6	11.07	11.44	11.23	11.77	11.51	14.11	17.03	9.61
7	12.23	12.49	12.51	13.03	12.72	15.65	19.23	10.68
8	13.35	13.48	13.59	14.28	13.86	17.46	21.60	11.93
9	14.47	14.43	14.67	15.54	15.02	19.46	24.28	13.01
10	15.63	15.57	15.73	16.85	16.18	21.68	25.97	14.07

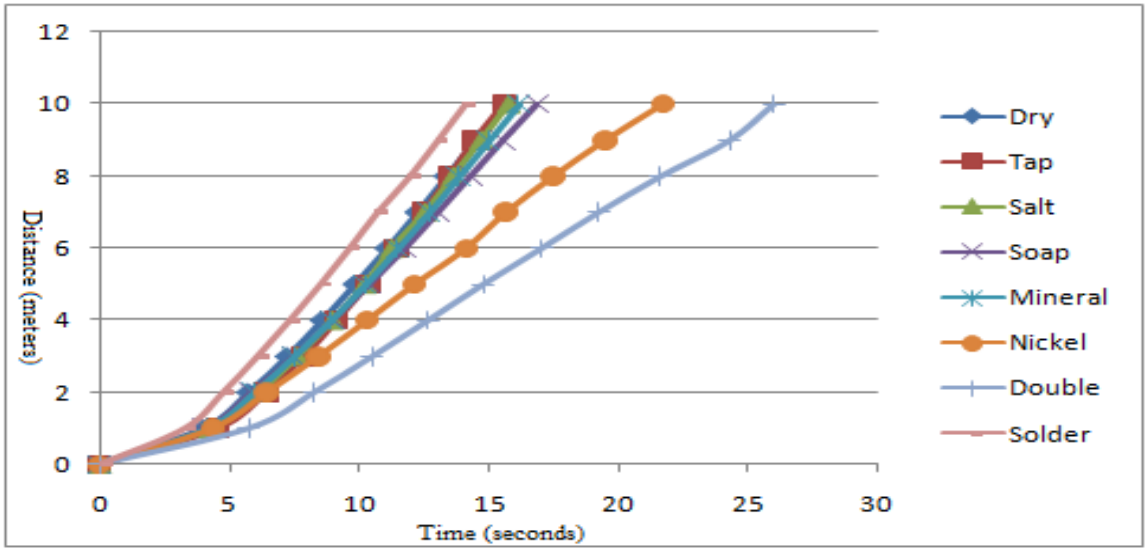

Figure 5.9: Time vs. distance graph for all physical results obtained during testing.

Since the graphs seem to have similar plots for each armature type, the same PSpice simulation may be used by altering the value of the contact resistance for each new armature. The contact resistance is changed from 0.75 Ω to 0.48 Ω in order to account for a solder armature. Figure 5.9 displays the results.

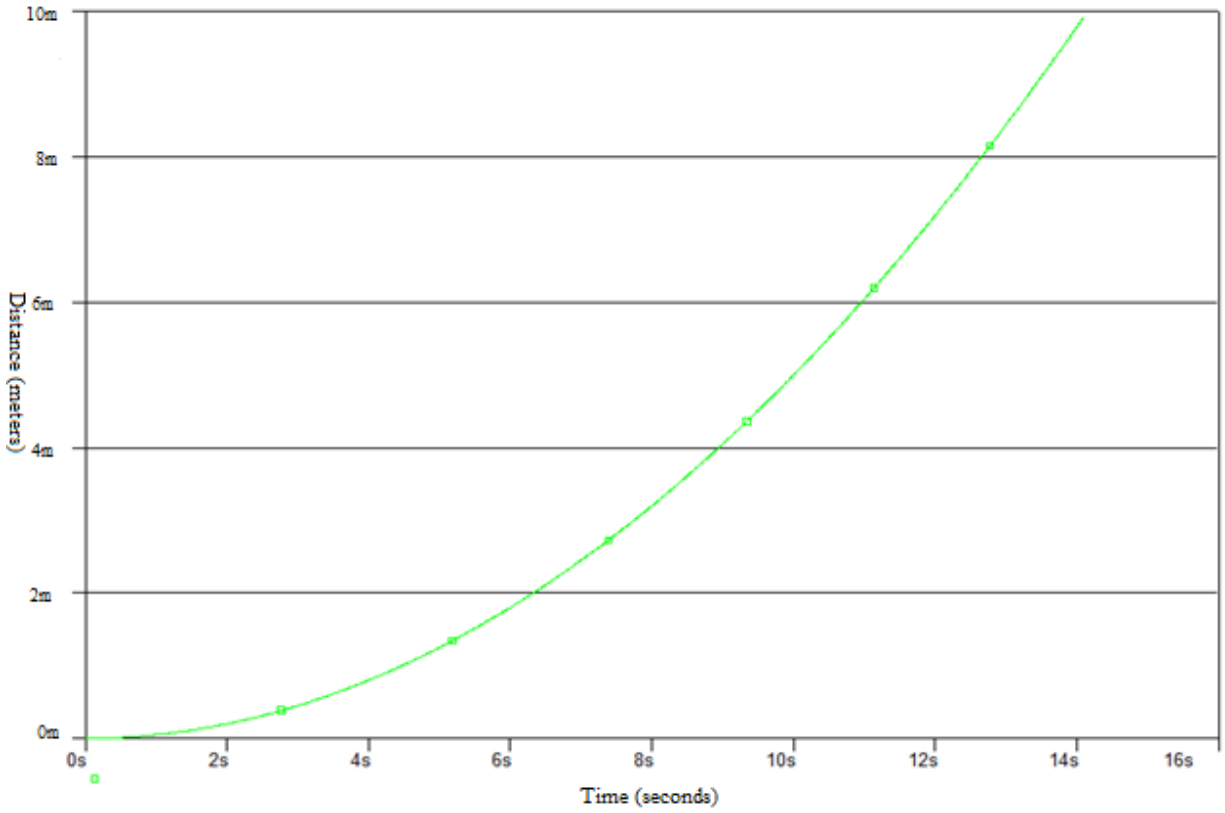

Figure 5.10: Time vs. distance graph for the solder simulation.

As before, the actual initial acceleration is smaller than the expected acceleration given by the simulation. However, both the simulation and the average measured values have an ending time of 14.06 seconds. The discrepancy between the initial times may be due to several factors, including friction and the effects of heat on the system. Since thermal energy will be produced while the battery is being discharged, this can produce a positive impact which speeds up the chemical reaction of the battery, allowing it to discharge more quickly. Therefore, the battery may not reach its full discharge capability until several seconds have passed. Also, the simulation assumes the magnetic field is perpendicular to the current flowing through the armature. Due to physical limitations, this will not always be true, so the induced Lorentz force may be slightly lower than expected.

Table 5.11: Solder simulation results

Distance (m)	1	2	3	4	5	6	7	8	9	10
Time (s)	4.4	6.3	7.7	8.9	10.0	11.0	11.8	12.6	13.4	14.1

Table 5.12: Solder physical results

Distance (m)	1	2	3	4	5	6	7	8	9	10
Time (s)	3.27	4.74	6.05	7.30	8.49	9.61	10.68	11.93	13.01	14.07

There are a number of variables which may affect the results and conclusions determined from these experiments. For example, each experimental run seems to be slightly faster whenever the batteries have been freshly charged. In other words, when the batteries are immediately removed once they have completed the recharging process, they seem to be able to expel current faster. As mentioned above, a higher temperature can have a positive effect on the discharging capabilities. The batteries normally have a warmer temperature soon after they have finished charging, so the additional heat will speed up the chemical reaction which produces the current. Sometimes the batteries are left to recharge overnight, so even though the battery has been fully replenished, it may have been allowed enough time to return to room temperature.

Alternatively, most conductors tend to become more resistive whenever the temperature is increased. The copper and solder armatures became warmer when some of the energy of the battery is expelled as thermal energy. Therefore, some of the subsequent tests may be slightly slower since the wire is warmer, and therefore less conductive. This effect should be minimal, however, and is therefore disregarded.

The thermal energy may actually improve the performance of the solder armature, however. Since the solder is very pliable, the heat will allow the solder to form to the shape of the magnets. This

will create a larger contact surface and the armature will be less likely to momentarily break contact with the magnet.

Another source of error may also include metallic dust or small metallic fillings. The magnets would attract these metallic pieces off the ground it is rolling across. When these become stuck to the magnet, the surface is not smooth and the armature contact may be disrupted. Also, if any metallic pieces go between the magnet and the battery, they will not be flush with each other. This will obstruct the apparatus from rolling smoothly, sometimes causing it to wobble.

Finally, different strengths of HCl solution are used to clean the copper wire. When the lubricant is tap water, soapy water, salt water, and mineral oil, a 5% HCl solution is used. The 'dry' experiments as well as the nickel-plated copper and double-turn formation are cleaned with a 37% HCl solution. The stronger solution might be able to remove more oxidation, but there is also a risk of stripping some of the copper.

The PSpice simulation developed for this thesis is able to display accurate results even when some experimental conditions are altered. By changing a few variables in the parameters table, a wide range of testing conditions may be simulated using this model. These variables include the size and mass of the magnet, washers, and batteries, the magnetic field strength, the length of the armature, and the total number of magnets used. When the magnet size parameters are input, the mass is automatically calculated for a neodymium magnet consisting of a NdFeB body. If another type of material is used, the density in the parameters table must be changed. For the different lubricants and armature materials, the contact resistance must be changed in the model. By controlling these variables, predictions may be made about the behavior of a homopolar motor. These predictions seem to be accurate based on physical data taken. Therefore, the PSpice simulation has successfully modeled the electromechanical properties of the homopolar motor and is able to predict its behavior.

References

[1] K&J Magnetics, Inc. http://www.kjmagnetics.com/proddetail.asp?prod=D82%2DN52&cat=168.

[2] "Michael Faraday," *WikiAnswers, Who2 Biography.* http://www.answers.com/topic/michael-faraday.

[3] "Homopolar Motor," *WikiAnswers,* http://www.answers.com/topic/homopolar-motor.

[4] "Energizer NH15-2500," Product Datasheet, *Energizer,* http://data.energizer.com/PDFs/nh15-2500.pdf

[5] R. Nave. "Friction Plot," *HyperPhysics.* http://hyperphysics.phy-astr.gsu.edu/hbase/frict2.html.

[6] "Hall Effect Measurements," *National Institute of Standards and Technology.* August 2007. http://www.eeel.nist.gov/812/hall.html.

[7] R. Nave. "Moment of Inertia," *HyperPhysics.* http://hyperphysics.phyastr.gsu.edu/hbase/mi.html.

[8] R.J. Thome, et al. "Homopolar Motor Technology Development," *Power Engineering Society Summer Meeting, 2002 IEEE,* vol. 1, pp. 260-264, 2002.

[9] C.A.Luongo, et al. "Next Generation More-Electric Aircraft: A Potential Application for HTS Superconductors," *IEEE/CSC & ESAS European Superconductivity News Forum,* No. 6, 2008.

[10] B. Williams. "Homopolar Generators," 2001. http://www.io.com/~bolie/Tech/Homopolar.html.

[11] E.A. Zobel. "Equations for Accelerated Motion," *Zona Land, Education in Physics and Mathematics,* 2006. http://id.mind.net/~zona/mstm/physics/mechanics/kinematics/EquationsforAcceleratedMotion/EquationsforAcceleratedMotion.htm

[12] "Homopolar Motor," *Dangerously Fun,* 2006. http://dangerouslyfun.com/homopolar-motor

[13] N. Chernyy. "How to Make a Homopolar Electric Motor," *ublog: Engineering from the trenches,* 2007. http://microblog.routed.net/2007/03/05/how-to-make-a-homopolar-electric-motor/.

[14] J. Douglas-Young. *Illustrated Encyclopedic Dictionary of Electronics*, Parker Publishing, Inc. West Nyack, NY, 1981, pp. 537-38.

[15] R.A. Serway, *Physics for Scientists and Engineers with Modern Physics*, Fourth Edition, Sauders College Publishing, Olrando, FL, 1996, pp. 34.

[16] "Examples of Magnetic Field Visualization Using Vizimag Software," *Visualizing Magnetic Fields.* http://www.vizimag.com/examples.htm.